Investigation Study of the Influence of Pole Numbers on Torque Density and Flux-Weakening Ability of Fractional Slot Concentrated Winding Wheel-Hub Machines

Zhu, Zichong ; Huang, Yunkai; Dong, Jianning; Peng, Fei

DOI
10.1109/ACCESS.2019.2924967

Publication date
2019

Document Version
Final published version

Published in
IEEE Access

Citation (APA)
Zhu, Z., Huang, Y., Dong, J., & Peng, F. (2019). Investigation Study of the Influence of Pole Numbers on Torque Density and Flux-Weakening Ability of Fractional Slot Concentrated Winding Wheel-Hub Machines. *IEEE Access*, *7*, 84918-84928. Article 8746231. https://doi.org/10.1109/ACCESS.2019.2924967

IEEE Access
Multidisciplinary | Rapid Review | Open Access Journal

Received June 4, 2019, accepted June 18, 2019, date of publication June 26, 2019, date of current version July 15, 2019.

Digital Object Identifier 10.1109/ACCESS.2019.2924967

Investigation Study of the Influence of Pole Numbers on Torque Density and Flux-Weakening Ability of Fractional Slot Concentrated Winding Wheel-Hub Machines

ZICHONG ZHU[1], (Student Member, IEEE), YUNKAI HUANG[1], JIANNING DONG[2], (Member, IEEE), AND FEI PENG[1], (Member, IEEE)

[1]School of Electrical Engineering, Southeast University, Nanjing 210096, China
[2]Faculty of Electrical Engineering, Mathematics, and Computer Science, Delft University of Technology, 2628CD Delft, The Netherlands

Corresponding author: Yunkai Huang (huangyk@seu.edu.cn)

This work was supported by the Natural Science Foundation of China under Grant 51777034.

ABSTRACT Fractional slot concentrated winding machines (FSCWMs) with the low operation speed and large diameter usually have a large number of poles and slots; thus, numerous pole/slot combinations are feasible. The common practice to choose pole/slot combinations by multiplying the basic combinations may neglect some competitive candidates. Taking 36-slot FSCWMs as examples, this paper investigates the influence of pole numbers on torque density and flux-weakening ability, the two most vital performances of wheel-hub machine. It is shown that the machines with pole number slightly less than the slot number have the highest torque densities. Each component of synchronous inductance is separately analyzed, and its variation against pole numbers shows obvious regularity. Machines with pole numbers larger than the slot numbers have an excellent flux-weakening ability due to the large inductance and small permanent magnet flux linkage. The measurements together with the finite element analysis results confirm that the stator leakage inductance contributes the most to the superior flux-weakening ability. The identical analysis is also performed on 54-slot and 81-slot FSCWMs, with similar regularities observed.

INDEX TERMS Flux weakening, fractional slot concentrated winding, pole number, torque density, wheel-hub machine.

I. INTRODUCTION

Fractional slot concentrated winding machine (FSCWM) is a good candidate for wheel-hub propulsion due to short end winding, high torque density and superior flux-weakening ability, especially when equipped with tooth coil winding [1]–[3].

For FSCWMs used in heavy vehicles with extremely low operation speed and large diameter, the number of poles and slots are usually large to increase torque output and improve heat dissipation in slot center [4]. As a result, hundreds of pole/slot combinations are feasible [5]. For examples, 36-slot FSCWM investigated in this paper has 12 viable pole number candidates, on the other hand, 56-pole FSCWM can match with 14 feasible slot numbers. When the slot number increases to 54 and 81, feasible pole number candidates even reach to 18 and 28 respectively. Machines with these pole/slot combinations have close fundamental frequencies, but different performance characteristics. It is difficult to determine the most suitable one simply based on the range of electrical frequency, which is a common practice when selecting pole number for integer slot distributed winding machines.

Many researches investigate the influence of pole/slot combinations on performances of FSCWM, including torque density [6], fault-tolerant ability [7], [8], cogging torque [9], rotor eddy current loss [10], unbalanced magnetic pull and torque ripple [11], [12]. These researches focus mainly on basic pole/slot combinations, e.g., 6/9 (6-pole 9-slot FSCWM with tooth coil winding, hereinafter), 8/9, 8/12, 10/9, 10/12, 14/12 and 14/15. According to the conclusions from these

The associate editor coordinating the review of this manuscript and approving it for publication was Bora Onat.

comparative studies, multiplying basic pole/slot combination is a common practice when selecting pole and slot numbers for FSCWMs with low speed and/or large diameter. For instance, 40/48 in [13] and 32/36 in [4] have four 10/12 and 8/9 basic combinations (unit motor) respectively. Nevertheless, these combinations derived from multiplying basic pole/slot combinations are not necessarily the best candidates. Some combinations, such as 28/36 [14], are rarely researched yet have better torque overload ability than common 32/36, as shown in Section III.

In addition, comparative studies of these basic pole/slot combinations are usually not fair enough, because the model machines are designed with various current densities, winding parameters, magnetic saturation and stator dimensions. Therefore, it is difficult to reasonably compare the flux-weakening ability of these combinations. There are few researches involved in this aspect [15], [16], especially regarding the influence of pole numbers.

Taking 36-slot FSCWMs as examples, this paper investigates the influence of pole numbers on torque density and flux-weakening ability, the two most vital performances of wheel-hub machine. FSCWMs with double layer winding and surface-mounted permanent magnet (SPM) rotor are focused due to shorter end winding, less magneto-motive force (MMF) harmonics and more sinusoidal back electromotive force (EMF) than alternatives with single layer winding or interior permanent magnet rotor [17].

The fundamental winding factor and open-circuit air-gap flux density are highly related to pole number. Consequently, the torque output which can be well predicted by the product of these two parameters shows obvious regularity against pole number. In this paper, apart from the analysis on winding factor and air-gap flux density, decomposition and calculation of synchronous inductance with finite element analysis (FEA) are undertaken to explore the effect of pole numbers on each inductance component and flux-weakening ability. In addition, the experimental measurement of inductances are used to validate the FEA results.

The main contribution of this paper is revealing the regularities that show the effect of pole numbers on torque density and flux-weakening ability. These regularities are valid for FSCWMs with identical slot number but different pole numbers. These regularities help to select the most suitable pole/slot combination or narrow down the searching space from hundreds of candidates in the early design stage, instead of simply multiplying the basic combinations. Moreover, by decomposing the synchronous inductance into different components, it found that the synchronous inductance is dominated by the stator leakage inductance, which improves the flux-weakening ability of FSCWM with SPM rotor, instead of the harmonic leakage inductance insisted in previous literatures [18]–[20]. In addition, calculation of the self- and mutual components of the stator leakage inductance by FEA concludes that the mutual component is non-negligible, which is usually ignored in most of analytical methods proposed by previous researches.

II. POLE NUMBER SELECTION

A. POLE NUMBER DETERMINATION

For a certain number of slots z, viable number of pole pairs p is first determined by torque production capacity, which can be measured by back EMF. Phase EMF E_{ph} and output torque T can be expressed as

$$E_{ph}=\sqrt{2}\pi f k_{wp} T_{ph} \Phi_{m1} = \sqrt{2}\pi f k_{wp} T_{ph} \frac{2}{\pi} B_{m1} \frac{2\pi r_{si}}{2p} l_{stk}, \quad (1)$$

$$\begin{aligned} T &= \frac{3E_{ph}I_m}{\omega} = \frac{3I_m}{2\pi f/p}\sqrt{2}\pi f k_{wp} T_{ph} \frac{2}{\pi} B_{m1} \frac{2\pi r_{si}}{2p} l_{stk} \\ &= 3\sqrt{2} r_{si} l_{stk} T_{ph} k_{wp} B_{m1} I_m, \end{aligned} \quad (2)$$

where $I_m, f, k_{wp}, T_{ph}, \Phi_{m1}, B_{m1}, r_{si}, l_{stk}$ and ω denote effective value of phase current, fundamental frequency, fundamental winding factor, total turns in series in each phase winding, fundamental flux per rotor pole, amplitude of fundamental open-circuit air-gap flux density, inner radius of stator core, axial length of stator lamination and rotor mechanical angular frequency respectively.

From (2), the torque constant k_T can be written as (3). When keeping l_{stk}, r_{si} and T_{ph} constant, k_T is proportional to k_{wp} and B_{m1}. Ideally, B_{m1} depends simply on the thickness and magnetic properties of permanent magnet (PM) and the effective air gap length. Actually, it decreases continuously when increasing pole number, as shown in the next section.

$$k_T = \frac{T}{I_m} = 3\sqrt{2} r_{si} l_{stk} T_{ph} \overbrace{k_{wp} B_{m1}}^{f(p)} \quad (3)$$

It can be seen that a large k_{wp} is a prerequisite to acquire large torque constant. Small k_{wp} value means winding current is not effectively used, and larger current or more coil turns are needed to compensate. k_{wp} is usually split into the distribution factor k_{dp} and the pitch factor k_{pp} when rotor and stator skew are not used, as in (4). k_{dp} depends not only on pole/slot combination but coil connection pattern (coil distribution for each phase winding). Normally, more than one connection patterns exist for a specific pole/slot combination [21]. It is hard to express k_{dp} as a uniform function of p and z. For certain coil connection pattern, k_{dp} is usually calculated through the star of slots diagram [22].

$$k_{wp} = k_{dp} k_{pp} \quad (4)$$

Fortunately, pitch factor k_{pp} is readily derived and can be written as a general function of p and z, as in (7), where h_c is coil pitch and equals to 1 for FSCWMs with tooth coil winding. τ and α_s denote the electrical pole pitch angle and slot pitch angle, given by (5) and (6). Thus, k_{pp} can be used to exclude some inappropriate pole number candidates. According to (7), $24 \leq 2p \leq 48$ is a prerequisite for keeping k_{pp} thus k_{wp} larger than 0.85 for 36-slot FSCWM ($z = 36$). Feasible pole numbers are 24, 26, 28, 30, 32, 34, 38, 40, 42, 44, 46 and 48.

$$\tau = \pi \quad (5)$$

$$\alpha_s = \frac{2p\pi}{z} \tag{6}$$

$$k_{pp} = \cos\left(\frac{\tau - h_c\alpha_s}{2}\right) = \cos\left(\frac{\pi}{2} - \frac{p\pi}{z}\right) = \sin\left(\frac{p\pi}{z}\right) \tag{7}$$

The method shown in [21] is used to determine the coil connection pattern that has largest k_{wp} for each pole/slot combination, while other patterns that produce smaller k_{wp} are not discussed in this paper. For example, coil connection patterns for 28/36 and 44/36 are illustrated in Fig. 1. Coil connection patterns of other combinations are not presented due to the space limit.

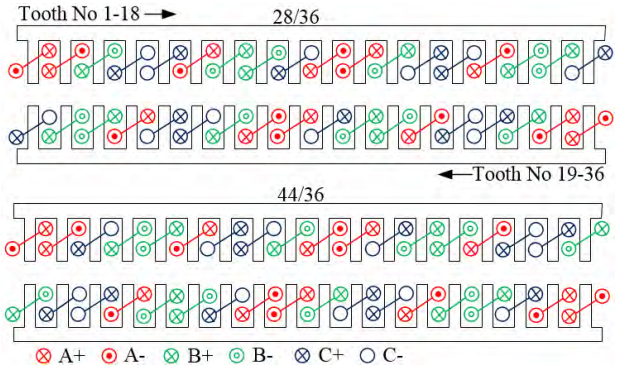

FIGURE 1. Coil connection patterns of 28/36 and 44/36.

B. INVESTIGATED MACHINE

To evaluate the influence of pole numbers on torque density and flux-weakening ability, 36-slot FSCWMs with 12 feasible pole numbers derived above are comparatively analyzed. Design specifications are listed in Table 1, and the rated torque-speed curve is shown in Fig. 2.

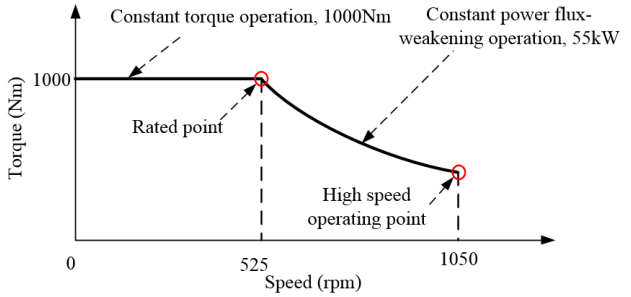

FIGURE 2. Torque-speed envelop of investigated wheel-hub machine.

TABLE 1. Specifications of 36-slot FSCWM for wheel-hub propulsion.

Rated speed n (rpm)	525	Maximal speed (rpm)	1050
Power P (kW)	55	DC bus voltage U_{dc} (V)	600
Rated torque (Nm)	1000	Overload torque (Nm)	2500
Rated current (A)	140	Overload current (A)	400
Rated current density (A/mm^2)	9.56	Cooling mode	Liquid

For fair comparisons, these 12 candidates use same stator core and are designed with identical rotor hub outer diameter and PM thickness. Main geometry parameters are schematically defined in Fig. 3. Pole-arc coefficient α_p of all candidates is fixed at 0.8, i.e., PM usages are identical. Stator yoke and rotor hub have relatively large thickness to avoid magnetic saturation. A 2mm thick nonmagnetic retaining sleeve is used to fix PMs onto the rotor hub and protect them from being destroyed by centrifugal force. The physical air gap δ_p is 1mm, selected according to machining and assembly requirements.

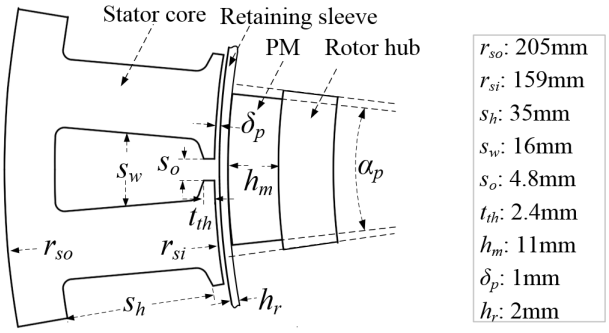

FIGURE 3. Definition of each dimension and its value.

Winding parameters are listed in Table 2. The number of turns per coil T_s is also identical for all candidates. To keep serial turns in each phase winding T_{ph} unchanged when altering pole number, parallel paths in each phase winding a is fixed at 1. Therefore, winding of different candidates can be obtained simply by reconnecting tooth coils to match various pole numbers.

TABLE 2. Design parameters of 36-slot FSCWMs with different poles.

$2p$	24	26	28	30	32	34	38	40	42	44	46	48
z	36											
T_s	8											
a	1											
T_{ph}	96 (12 coils in series)											
q	1/2	6/13	3/7	2/5	3/8	6/17	6/19	3/10	2/7	3/11	6/23	1/4

It can be seen from Table 2 that feasible pole numbers distribute symmetrically on both sides of the slot number. The two candidates with pole numbers distributing symmetrically in the table have exactly identical winding connection pattern, as shown in Fig. 1, while only phase sequence is changed. Fig. 4 gives the spectra of 3-phase MMF of 36-slot FSCWMs with different poles. It can be observed that each pole/slot combination has a counterpart that shares the same MMF spectrum. For example, 28/36 and 44/36 have identical coil connection pattern and MMF waveform, thus MMF spectrum, but they use the 14th and 22nd space harmonics (in mechanical reference) as the fundamental harmonic respectively. Since the 14th and 22nd harmonics have different rotation directions, phase sequences of these two candidates are opposite. This is also the case for other machines. Machines that use higher order harmonics (in the dotted ellipse) have different torque density and flux-weakening

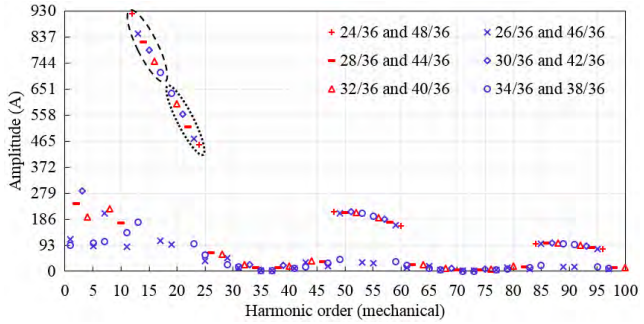

FIGURE 4. Spectra of the MMF of 36-slot FSCWMs when excited by the rated current (up to the 100th space harmonic).

ability compared with that using lower order harmonics (in the dashed ellipse), as discussed in the following sections.

III. INFLUENCE ON TORQUE DENSITY

Since the number of slots per pole per phase q is small in FSCWMs, as in Table 2, distribution factor k_{dp} is large for all combinations (k_{dp} >0.95). Meanwhile, the difference of k_{dp} between various combinations is not as obvious as that of pitch factor k_{pp}. Therefore, fundamental winding factor k_{wp} shows nearly consistent variation trend with k_{pp}. Calculated k_{wp} is shown in Fig. 5 (a). It can be seen that combinations with $2p$ close to z have larger k_{wp} that may have larger torque constant, according to (3).

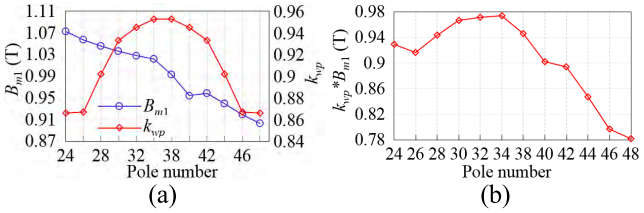

FIGURE 5. Variations of B_{m1} and k_{wp} when altering pole number. (a) B_{m1} and k_{wp}. (b) $B_{m1} * k_{wp}$.

Another factor that affects torque constant is the fundamental open-circuit air-gap flux density B_{m1}. As mentioned above, ideally, B_{m1} is independent of pole number. Nevertheless, in fact, it is significantly influenced by pole number due to inter-pole flux leakage. As shown in Fig. 6, more PM flux leakage is produced in 48/36 than 24/36, which inevitably results in a smaller B_{m1}. In order to consider the effect of flux leakage and local magnetic saturation, FEA is used to calculate B_{m1}, as shown in Fig. 5 (a). Clearly, B_{m1} tends to decrease when using more poles.

The product of k_{wp} and B_{m1} is shown in Fig. 5 (b), where B_{m1} is calculated by 2-D FEA. Since B_{m1} decreases nearly monotonously and k_{wp} has maximal values in the middle of pole array, the highest torque production does not appear in candidates with $2p$ closest to z, i.e., 34/36 and 38/36, but in candidates whose pole numbers are slightly less than those, e.g., 30/36, 32/36 and 34/36.

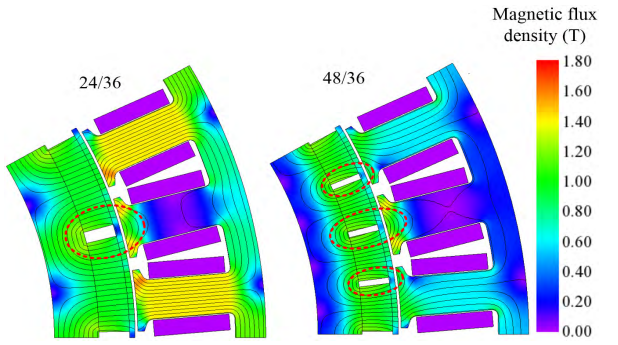

FIGURE 6. Inter-pole flux leakage at open circuit.

Fig. 7 shows semi-analytically and numerically calculated torques for all machines. Semi-analytical results are calculated using (2), where B_{m1} is obtained by 2-D FEA. Convex curves illustrate that under both rated and overload operating points, maximal torques appear in machines that have $2p$ slightly less than z. An exception is 26/36, its B_{m1} decreases significantly compared with 24/36, while k_{wp} does not have obvious increment. As a result, torque output of 26/36 is lower than that of 24/36. In addition, machines with $2p > z$ show inferior torque production capability considering large inter-pole flux leakage.

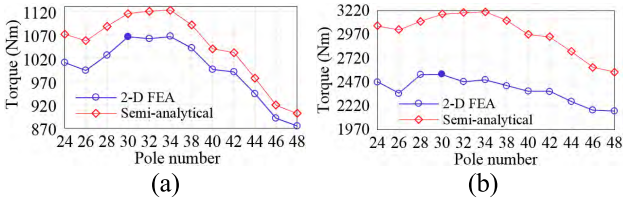

FIGURE 7. Torque output of 36-slot FSCWMs with different poles. (a) Rated point-140A. (b) Overload condition-400A.

It is noteworthy that the torque variation profile calculated from FEA shows excellent agreement with semi-analytical result at the rated point, as shown in Fig. 7 (a). This means (2) is effective to compare torque output of FSCWMs with different poles. However, under the overload condition, it is not as accurate as that at the rated point. As in Fig. 7 (b), the maximal torques appear in candidates with fewer poles, such as 28/36 and 30/36, which means that a certain degree of pole number reduction benefits overload ability.

IV. SYNCHRONOUS INDUCTANCE CALCULATION

Accurate inductance calculation is essential for flux-weakening ability analysis, the synchronous inductance L_s determines characteristic current I_{ch} and flux-weakening ratio ζ, which are usually used to evaluate the flux-weakening ability, as in (8) and (9).

$$I_{ch} = \frac{\psi_m}{L_s} \tag{8}$$

$$\zeta = \frac{L_s i_d}{\psi_m} \tag{9}$$

where ψ_m is the PM flux linkage of phase winding.

Although the total inductance L_s can be calculated accurately by FEA, analytical calculation and decomposition of it are necessary to explore the effect of pole numbers and determine the contribution of each component to flux-weakening ability. This section calculates each component of L_s analytically, and FEA is used to validate these results. Larger errors are detected in these analytical methods that are widely used in literatures, which are not reported previously. The next section gives measured inductances to validate the calculated results.

Corresponding to each armature flux flow path, L_s is separated into several components as

$$L_s = L_g + L_\sigma = \overbrace{L_m + L_\delta}^{L_g} + \overbrace{L_{ti} + L_{sl} + L_{ew}}^{L_\sigma}, \quad (10)$$

where L_g, L_σ, L_m, L_δ, L_{ti}, L_{sl} and L_{ew} are air gap inductance, stator leakage inductance, magnetizing inductance, harmonic leakage inductance, tooth tip leakage inductance, slot leakage inductance and end winding inductance respectively.

A. STATOR LEAKAGE INDUCTANCE

This part focuses on L_{ti}, L_{sl} and L_{ew}. The sum of them, the stator leakage inductance L_σ, corresponds to the flux that traverses various parts of the stator core except the air gap.

Each component of L_σ is analytically calculated for FSCWM and integer slot distributed winding machine that have same pole number and fundamental flux linkage in [23], which assumes that L_σ depends only on the number of turns per coil T_s and slot dimensions, yet is independent of coil connection pattern. Other researches, e.g., [20] and [24], also consider L_σ related merely to T_s and stator geometry parameters, such as tooth tip height t_{th}, slot opening s_o, slot width s_w, slot depth s_h, coil span t_w and mean length of coil end l_{ew}, as shown in Fig. 3. Analytical formulas of L_{ti}, L_{sl} and L_{ew} in these literatures base on corresponding permeance functions λ_{ti}, λ_{sl} and λ_{ew} that are functions of above geometry parameters. Generally, they are written as (11), these permeance functions are derived from ideal slot shape and show poor accuracy in real machines, so they are not listed in detail here.

$$\begin{aligned} L_\sigma &= L_{ti} + L_{sl} + L_{ew} = 12\mu_0 T_s^2 (\lambda_{ti} + \lambda_{sl} + \lambda_{ew}) \\ &= 12\mu_0 T_s^2 \begin{pmatrix} \lambda_{ti}(l_{stk}, s_o, t_{th}) \\ +\lambda_{sl}(l_{stk}, s_h, s_w, s_o, t_{th}) \\ +\lambda_{ew}(l_{ew}, t_w) \end{pmatrix} \end{aligned} \quad (11)$$

In addition, (11) takes only self-inductance into account. Mutual coupling between each coil is assumed to be negligible in many literatures [20], [23]. Permeance function models that accounting for mutual coupling are rare in existing literatures [16]. In fact, the mutual component of L_σ is significant and should not be ignored. In addition, both self-inductance $L_{\sigma s}$ and mutual inductance $L_{\sigma m}$ have tight relationship with coil connection pattern, i.e., pole number.

To clearly present the relationships, L_σ is calculated by imposing symmetry boundary conditions on stator inner surface in 3-D FEA models [25], [26]. These conditions prohibit armature flux from entering the air gap and constrain it flowing parallel to these faces, as in Fig. 8. Fig. 9 gives calculated flux linkages when feeding only sinusoidal A-phase current of 140A (results of 38/36, 40/36, 42/36, 44/36, 46/36 and 48/36 are not plotted because the flux linkage of them are identical to their counterparts that share same coil connection pattern).

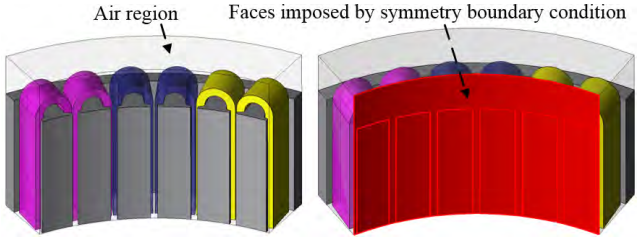

FIGURE 8. 3-D FEA partial model used to calculate stator leakage inductance (30/36).

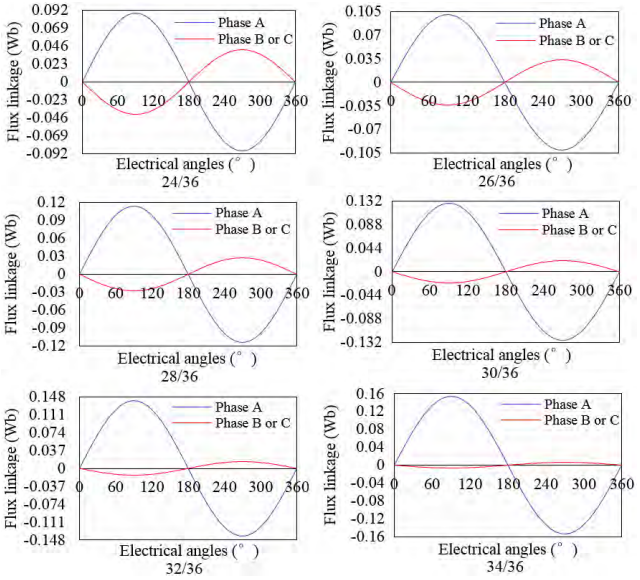

FIGURE 9. Flux linkages in each phase winding when feeding 140A current into phase A.

It can be seen that the mutual flux linkages are non-negligible and the ratio of B-phase and A-phase flux linkages changes dramatically in different machines. Fig. 10 (a) and (b) show resultant $L_{\sigma s}$ and $L_{\sigma m}$ calculated from flux linkages using (12) and (13), where ψ_a, ψ_b and i_a denote A-phase flux linkage, B-phase flux linkage and A-phase current respectively. Fig. 10 (c) shows L_σ. Fig. 10 (d) gives the ratio of $L_{\sigma m}$ and L_σ.

$$L_{\sigma s} = \psi_a / i_a \quad (12)$$

$$L_{\sigma m} = \psi_b / i_a \quad (13)$$

It can be seen from Fig. 10 (a) that $L_{\sigma s}$ increases if more poles are used when $2p < z$. Machines with $2p$ closest to z have the maximum $L_{\sigma s}$ of 1.15mH, i.e., 34/36 and 38/36. However, $L_{\sigma m}$ shows a totally different trend, as shown

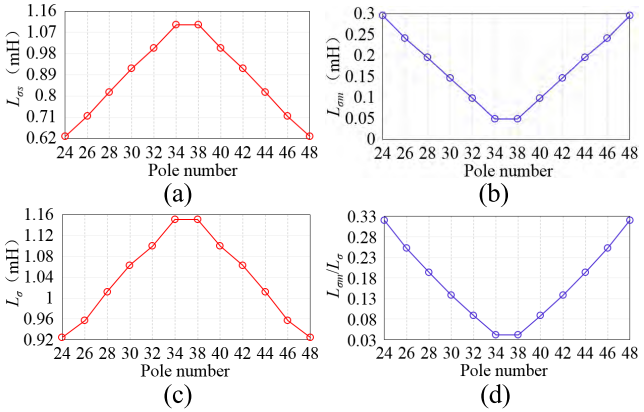

FIGURE 10. Variations of $L_{\sigma s}$, $L_{\sigma m}$ and L_{σ} against pole numbers. (a) $L_{\sigma s}$. (b) $L_{\sigma m}$. (c) L_{σ}. (d) $L_{\sigma m}/L_{\sigma}$.

in Fig. 10 (b). It has minimum value 0.048mH in these two machines. This can be observed intuitively from mutual flux linkages in Fig. 9, where ψ_b decreases continuously when $2p$ increases from 24 to 34. In 24/36, ψ_b reaches half of ψ_a, but only 4.37% of ψ_a in 34/36. The ratio of $L_{\sigma m}$ and L_{σ} decreases from 0.33 to 0.042 when $2p$ increases from 24 to 34. That is, machines with $2p$ close to z have larger $L_{\sigma s}$ and smaller $L_{\sigma m}$. These features are attractive when considering fault-tolerant ability.

L_{σ} is *dominated* by $L_{\sigma s}$ and has maximum value in machines with $2p$ closest to z, despite where $L_{\sigma m}$ is minimum. More importantly, $L_{\sigma s}$, $L_{\sigma m}$ and L_{σ} are related to coil connection pattern. Analytical calculation using (11) that ignores these relations shows poor accuracy and is invalid for real machines.

B. AIR-GAP INDUCTANCE

Armature flux that traverses air gap is represented by L_g. It is usually split into two parts: magnetizing inductance L_m and harmonic leakage inductance L_{δ}, as (14).

$$L_g = L_m + L_{\delta} \tag{14}$$

Since the number of slots per pole per phase q is small in FSCWMs, MMFs produced by tooth-coil winding are far from sinusoidal and contain rich harmonics. The first term of L_g corresponds to the fundamental of armature field that interacts with rotor field to produce a constant torque. L_{δ} corresponds to all harmonic components, and a large L_{δ} may signify rotor eddy current loss due to these harmonics.

L_m and L_{δ} are usually calculated using winding functions [27], [28], which intrinsically describe how winding coils are arranged [29]. Mutual inductance L_{ab} between phase A and B can be expressed as

$$L_{ab} = \frac{\mu_0 r_{si} l_{stk}}{\delta} \int_0^{2\pi} N_a(\theta) N_b(\theta)\, d\theta, \tag{15}$$

where $N_a(\theta)$ and $N_b(\theta)$ are winding functions of phase A and B, θ is the angular measure along the air gap (in mechanical reference), δ is the length of effective air gap (the sum of physical air gap, the thickness of retaining sleeve, and the thickness of PM).

Self-inductance L can be obtained using (15) as well if replace $N_b(\theta)$ with $N_a(\theta)$. Winding functions are usually decomposed to Fourier series for harmonic analysis and written as

$$\begin{aligned} N_a(\theta) &= \frac{2T_{ph}k_{w1}}{\pi}\cos(\theta+\varphi_1) + \frac{2T_{ph}k_{w2}}{2\pi}\cos(2\theta+\varphi_2) \\ &\quad + \frac{2T_{ph}k_{w3}}{3\pi}\cos(3\theta+\varphi_3) + \ldots \\ &= \frac{2T_{ph}}{\pi}\sum_{\nu=1,2,3,\ldots}^{\infty}\frac{k_{w\nu}}{\nu}\cos(\nu\theta+\varphi_{\nu}), \end{aligned} \tag{16}$$

where $k_{w\nu}$ denotes the winding factor of the ν^{th} harmonic. φ_{ν} is the phase of the ν^{th} harmonic, which can only be 0 or π, because $N_a(\theta)$ is even symmetrical. Upon integrating, self-inductance L is solved as (17).

$$L = \frac{4\mu_0 r_{si} l_{stk} T_{ph}^2}{\pi\delta}\sum_{\nu=1,2,3,\ldots}^{\infty}\frac{k_{w\nu}^2}{\nu^2} \tag{17}$$

Self- and mutual components of L_g can be calculated together by replacing $N_b(\theta)$ in (15) with synthesized 3-phase winding function $N_{abc}(\theta)$, as given in (18).

$$L_g = \frac{\mu_0 r_{si} l_{stk}}{\delta}\int_0^{2\pi} N_a(\theta) N_{abc}(\theta)\, d\theta \tag{18}$$

In a three phase machine of basic pole/slot combination, windings are symmetrically arranged by $2\pi/3$ radians. Therefore, triple harmonics are cancelled out from synthesized winding function $N_{abc}(\theta)$. Accordingly, for the machine whose pole/slot combination derived from multiplying the basic combination, the harmonics corresponding to these triple harmonics are eliminated. For example, the 3rd and 6th harmonics of $N_a(\theta)$ of 8/9 are eliminated in $N_{abc}(\theta)$. Correspondingly, the 12th and 24th harmonics are excluded from $N_{abc}(\theta)$ of 32/36 that contains four basic 8/9 combinations. These harmonics correspond to zero-sequence inductance, which has no effect on flux-weakening analysis, yet should be taken into account in fault analysis. Thus, L_g is given as (19), where t is the number of basic combinations contained in certain pole/slot combination.

$$L_g = \frac{3}{2} * \frac{4\mu_0 r_{si} l_{stk} T_{ph}^2}{\pi\delta}\sum_{\substack{\nu=1,2,3,\ldots \\ \nu\neq t*3k,\, k=1,2,3,\ldots}}^{\infty}\frac{k_{w\nu}^2}{\nu^2} \tag{19}$$

The multiplier 3/2 in (19) represents the contribution of mutual inductance, as the amplitude of the remained harmonics ($\nu \neq t*3k$) are multiplied by 3/2 due to phase coupling. Therefore, L_m, L_{δ} and the ratio of them, referenced as the harmonic leakage factor σ, are given as (20)-(22). Since the term in the bracket is identical for all 12 candidates, L_m and L_{δ}

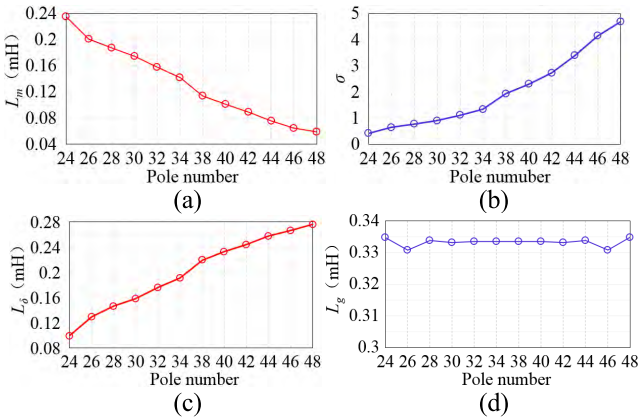

FIGURE 11. Variations of L_m, σ, L_δ and L_g against pole numbers. (a) L_m. (b) σ. (c) L_δ. (d) L_g.

vary with winding factors and harmonic spectra, which are tightly related to pole numbers.

$$L_m = \left(\frac{6\mu_0 r_{si} l_{stk} T_{ph}^2}{\pi \delta}\right) \frac{k_{wp}^2}{p^2} \tag{20}$$

$$L_\delta = \left(\frac{6\mu_0 r_{si} l_{stk} T_{ph}^2}{\pi \delta}\right) \sum_{\substack{\nu = 1,2,3,\ldots,\nu \neq p,\\ \nu \neq t*3k, k = 1,2,3,\ldots}}^{\infty} \frac{k_{w\nu}^2}{\nu^2} \tag{21}$$

$$\sigma = \frac{L_\delta}{L_m} = \sum_{\substack{\nu = 1,2,3,\ldots,\nu \neq p,\\ \nu \neq t*3k, k = 1,2,3,\ldots}}^{\infty} \frac{p^2 k_{w\nu}^2}{k_{wp}^2 \nu^2} \tag{22}$$

Fig. 11 shows analytically calculated L_m, σ, L_δ and L_g using (20)-(22), where L_δ and σ are counted up to the 200$^{\text{th}}$ space harmonic. From Fig. 11 (a), L_m decreases when more poles are used, with a drop from 0.235mH to 0.059mH when $2p$ doubles from 24 to 48. L_m of 48/36 is only a quarter of that of 24/36 since these two machines have identical MMF spectrum and harmonic winding factor, but different fundamental harmonic orders.

Opposite trends are observed in the variation of σ and L_δ, shown in Fig. 11 (b) and (c). They both increase significantly when using more poles. σ increases from 0.42 to 4.69 while L_δ increases from 0.099mH to 0.275mH. Starting from 32/36, L_δ becomes larger than L_m. Approximately, L_g is dominated by L_m in machines with $2p < z$. But when $2p > z$, L_δ takes a larger proportion. In addition, it is noteworthy that the sum of L_m and L_δ, i.e., L_g, is nearly constant regardless of pole numbers, as in Fig. 11 (d).

Analytical calculation using winding functions bases on some assumptions and hypotheses:

1. ignoring the slotting effect,
2. assuming stator core and rotor hub infinitely permeable, MMFs drop only on the effective air gap δ,
3. δ is considered to be small and armature flux traverses it radially, then enters the rotor hub.

The first two assumptions may cause minor errors and can be modified by using more complicated models or correction factors [27]. Nevertheless, this is not the case for the third, particularly in machines with SPM rotor. Actually, not all armature flux enters the rotor hub. Part flux bypasses it and returns to the stator core directly, as in Fig. 12. As a result, magnetic circuit permeance and L_g are inevitably underestimated. For instance, armature field distribution on the stator inner surface of 28/36 and its spectrum are shown in Fig. 13. It can be seen that the amplitude of nearly all harmonics are increased due to a decreased effective air gap length, which means the armature reaction is enhanced and a larger L_g is produced, compared with winding function analysis.

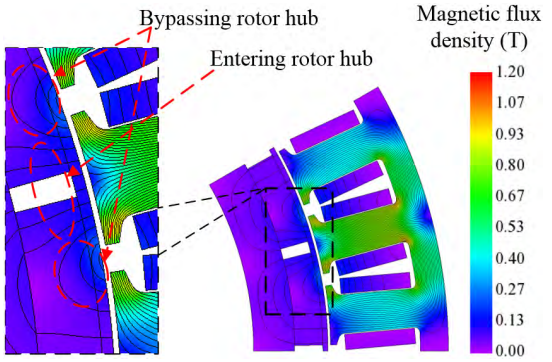

FIGURE 12. Armature field distribution of 24/36 with all three phases excited.

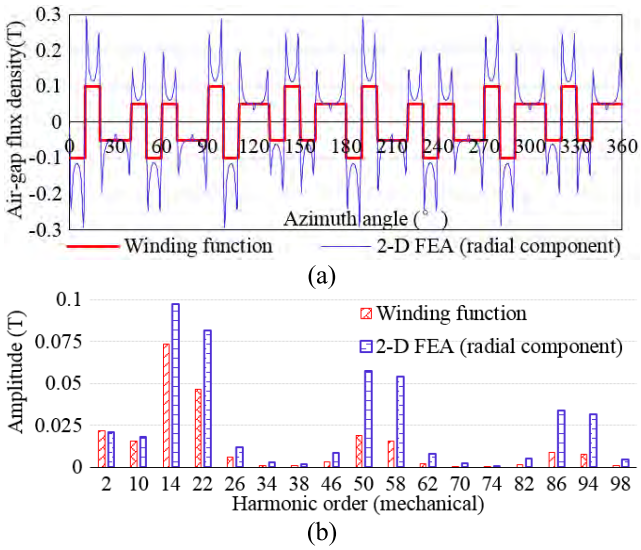

FIGURE 13. Armature field distribution (PMs are disabled) and its spectrum of 28/36. (a) Armature flux density in the air gap B_{ar}. (b) Spectrum of B_{ar}.

To improve accuracy, 3-D FEA is used to calculate L_g. Unlike what has been done for stator leakage inductance L_σ in Fig. 8, direct calculation of L_g by imposing symmetry

boundary conditions to hinder stator leakage flux causes large error. In this paper, L_g is obtained by subtracting L_σ from L_s, according to (10). Fig. 14 shows L_s from 3-D FEA and resultant L_g. Comparing Fig. 14 (a) with Fig. 11 (d), L_g increases about 50% when considering true flow paths of armature flux with FEA. It can be seen from Fig. 10 (c) and Fig. 14 (a), L_g shows the same variation trend as L_σ, and machines with $2p$ close to z also have larger L_g.

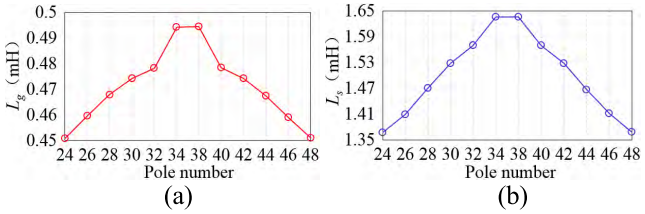

FIGURE 14. L_g and L_s calculated by 3-D FEA. (a) L_g. (b) L_s.

Total inductance L_s is shown in Fig. 14 (b). It is generally concluded in many papers [18]–[20] that L_s is dominated by the harmonic leakage inductance L_δ in FSCWM. However, comparing Fig. 10 (c) with Fig. 14 (a), L_s of FSCWM with SPM rotor is actually dominated by the stator leakage inductance L_σ due to small coil pitch and large effective air gap, instead of L_δ.

V. MEASUREMENT OF INDUCTANCE

It is impossible to constrain armature flux flow paths in the experimental measurements like that in FEA. In addition, the standard method recommended by IEEE 115-2009 to measure the stator leakage inductance L_σ with rotor removed test ignores the effect of harmonic leakage inductance. This method is applicable for integer slot distributed winding machines but shows poor accuracy when extending it to FSCWMs [20]. Thus far, it is difficult to distinguish each component from measured inductance.

In a compromise, indirect validations on calculated results are performed by measuring the total inductance L_s with and without permeable rotor hub. The 36-slot stator with tooth coils is fabricated to measure the inductance of machines with different pole numbers, as in Fig. 15. Each coil has two terminals for convenience of changing the coil connection patterns for various pole/slot combinations. Thus, all measurements use the same stator core and rotor hub, which helps to eliminate inherent machining errors and magnetic property difference.

Two measurements are carried out-one is performed when removing the rotor, while another with a permeable rotor hub. The calculated (3-D FEA) and measured synchronous inductances with LCR meter are listed in Table 3. The result for machines with $2p > z$ are not shown since they are identical to their counterparts.

The errors between measured and calculated results are about 4%, which may result from the difference of magnetic properties of the stator core in the FEA model and prototype. From measured results, the maximum L_s also appears

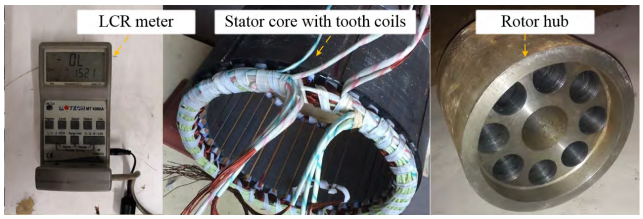

FIGURE 15. Stator with 36 tooth coils and the permeable rotor hub without PMs assembled.

TABLE 3. Synchronous inductances for 36-slot FSCWMs.

Machine	L_s (mH), Calc, no rotor hub	L_s (mH), Meas, no rotor hub	L_s (mH) Calc, with rotor hub	L_s (mH) Meas, with rotor hub
24/36	1.31	1.27	1.37	1.34
26/36	1.36	1.32	1.42	1.39
28/36	1.41	1.37	1.48	1.44
30/36	1.48	1.43	1.53	1.50
32/36	1.53	1.49	1.58	1.54
34/36	1.60	1.55	1.64	1.60

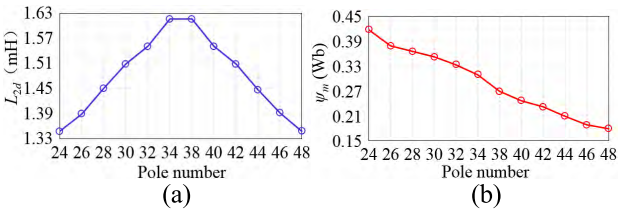

FIGURE 16. Synchronous inductance L_{2d} and open-circuit phase flux linkage ψ_m.

in machines with $2p$ closest to z, which is consistent with the calculated result. When with the rotor hub, measured L_s increases from 1.34mH to 1.60mH as $2p$ increases from 24 to 34. This increment owes much to a larger stator leakage inductance L_σ, rather than air-gap component L_g, as presented in section IV. In addition, L_s measured with the rotor hub has little increment compared with that when rotor hub is removed. This implies that little armature flux enters the rotor hub, and inductance corresponding to this part of flux is relatively small compared with others.

VI. FLUX-WEAKENING ABILITY ANALYSIS

The synchronous inductance calculated by 2-D FEA L_{2d} is shown in Fig. 16 (a). It contains all components of L_s except end winding inductance L_{ew}, as in (23). Therefore, L_{ew} can be indirectly calculated by differentiating L_{2d} and L_s from 3-D FEA, given as (24). Resultant L_{ew} is equal to 0.02mH for all 12 candidates. Clearly, L_{ew} is negligible compared with other components of L_s since FSCWMs have short end winding and non-overlapping coil arrangement. Therefore, L_{ew} is excluded when comparing flux-weakening ability of machines with different pole numbers, as in (25) and (26).

$$L_{2d} = L_m + L_\delta + L_{ti} + L_{sl} \tag{23}$$

$$L_{ew} = L_s - L_{2d} \tag{24}$$

$$I_{ch} = \frac{\psi_m}{L_{2d}} \tag{25}$$

$$\zeta = \frac{L_{2d} i_d}{\psi_m} \tag{26}$$

Another factor that determines flux-weakening ability is PM flux linkage ψ_m, given by (27). ψ_m is inversely proportional to the number of pole pairs p when assuming open-circuit air-gap flux density B_{m1} is constant for all 12 machines. In fact, B_{m1} decreases continuously when using more poles, as shown in Fig. 5 (a). As a result, ψ_m decreases monotonously since serial turns T_{ph} is kept constant for all machines, as shown in Fig. 16 (b).

$$\psi_m = k_{wp} T_{ph} \Phi_{m1} = k_{wp} T_{ph} \frac{2}{\pi} \pi r_{si} l_{stk} \frac{B_{m1}}{p} \tag{27}$$

Characteristic current I_{ch} and flux-weakening ratio ζ calculated using (25) and (26) are shown in Fig. 17. It can be seen that machines with a larger number of poles have smaller I_{ch} due to a smaller ψ_m, although L_{2d} has maximum value in combinations with $2p$ close to z. Meanwhile, ζ increases significantly when using more poles. For some machines, ζ is even larger than 1, such as 46/36 and 48/36. This means that FSCWMs with $2p > z$ have excellent flux-weakening ability, while integer slot distributed winding machine with SPM rotor is usually considered inappropriate when emphasizing this performance.

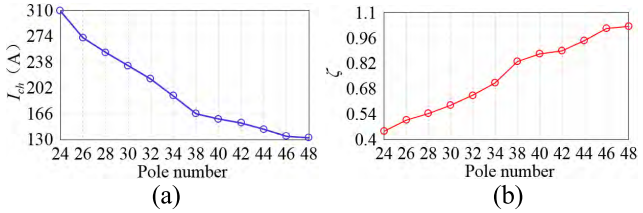

FIGURE 17. Characteristic current I_{ch} and flux-weakening ratio ζ.

Most importantly, comparing Fig. 10 (c) with Fig. 14 (a), air-gap inductance L_g is only about half of the stator leakage inductance L_σ. In other words, L_{2d} is dominated by L_σ and the excellent flux-weakening ability owes to it, rather than the harmonic leakage inductance L_δ suggested in [19], [20].

From above analysis, it seems that a machine with maximum pole number is preferred for flux-weakening operation. However, considering torque production inferiority, it may not be the best candidate. Since stator core loss is only about 1/12 of winding copper loss (e.g., these two kinds of loss are 268.3W and 3105.9W for 30/36 at rated operating point), machine that applies minimum current to reach the given torque and speed is preferred. Input current I_m is determined according to the procedures shown in Fig. 18, where U_{max} is the maximum output phase voltage of inverter with given dc bus voltage U_{dc}. With a 600V U_{dc}, normal 6-transistor inverter is able to produce 345V U_{max} with space vector pulse width modulation.

Q-axis current i_q required to obtain the rated torque during constant torque operation and corresponding critical speed

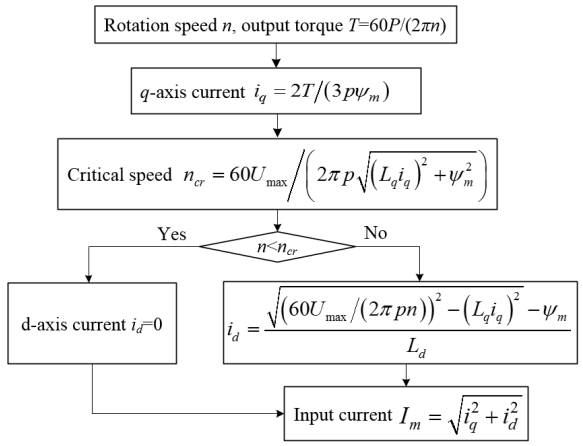

FIGURE 18. Procedures to calculate the minimum input current I_m.

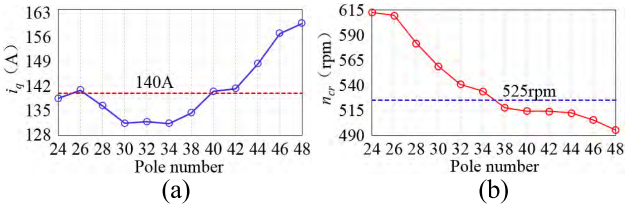

FIGURE 19. Q-axis current i_q and corresponding critical speed n_{cr}.

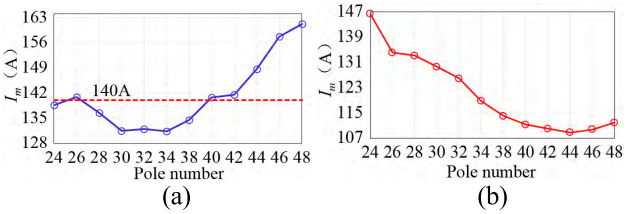

FIGURE 20. Input current I_m. (a) Rated operating point. (b) High-speed operating point.

n_{cr} are shown in Fig. 19. It can be seen that to produce rated torque, 30/36, 32/36 and 34/36 need the least currents. When $2p > z$, I_m increases monotonously. 44/36, 46/36 and 48/36 need much more current than others due to relatively small ψ_m. Moreover, they have low critical speeds due to larger pole numbers, as in Fig. 19 (b). Machines with $2p > z$ have critical speeds lower than the rated value 525rpm, which means flux-weakening control and d-axis current i_d are necessary to meet the speed requirement. The existence of i_d further increases the amplitude of I_m, and thus produces more copper loss. Resultant I_m at rated operating point (1000Nm, 525rpm) and high-speed operating point (500Nm, 1050rpm) are shown in Fig. 20.

At the high-speed operating point, the minimum I_m appears in 44/36. For machines with fewer poles, larger i_d is necessary to weaken PM field, while for machines with more poles, larger i_q is used to produce the required torque due to smaller ψ_m. Therefore, for other operating points of flux-weakening operation, the minimum I_m always appears in

machine with $34 \leq 2p \leq 44$. Generally speaking, machines with $2p$ slightly larger than z are recommended when emphasizing flux-weakening ability.

It is noteworthy that the maximal torque density and optimal flux-weakening ability do not appear in the same design candidate, but in a range of $30 \leq 2p \leq 44$, the lower and upper limits correspond to the maximal torque density and the optimal flux-weakening ability respectively. To determine the combination that has the highest operation efficiency, driving cycle of the electrical vehicle and control strategies should be taken into account. This will be presented in future work.

VII. CONCLUSION

For FSCWMs with a large number of poles and slots, hundreds of pole/slot combinations are feasible. Simply multiplying the basic combinations may miss some competitive candidates. Taking 36-slot FSCWMs as examples, this paper investigates the influence of pole numbers on torque density and flux-weakening ability of wheel-hub machines.

By imposing constraints on the comparative studies, it is found that some conclusions and calculation methods in previous literatures are not valid or show poor accuracy. For example, stator leakage inductance contributes the most to the superior flux-weakening ability of FSCWM with SPM rotor, instead of previously thought harmonic leakage inductance. Experimental measurements of total inductance have confirmed this conclusion. More importantly, the influence of pole numbers show obvious regularities, which are also observed in 54-slot and 81-slot FSCWMs with various pole numbers. The analysis results obtained help to determine the preferred combination or narrow down the searching space in the early design stage.

The influence of pole numbers on other performances, such as rotor eddy current loss, iron loss, and the effect of slot numbers on performance of FSCWMs with identical pole number but different slot numbers will be presented in future work.

REFERENCES

[1] J. Wang, X. Yuan, and K. Atallah, "Design optimization of a surface-mounted permanent-magnet motor with concentrated windings for electric vehicle applications," *IEEE Trans. Veh. Technol.*, vol. 62, no. 3, pp. 1053–1064, Mar. 2013.

[2] G. Hong, T. Wei, and X. Ding, "Multi-objective optimal design of permanent magnet synchronous motor for high efficiency and high dynamic performance," *IEEE Access*, vol. 6, pp. 23568–23581, 2018.

[3] A. M. El-Refaie, T. M. Jahns, P. J. McCleer, and J. W. McKeever, "Experimental verification of optimal flux weakening in surface PM Machines using concentrated windings," *IEEE Trans. Ind. Appl.*, vol. 42, no. 2, pp. 443–453, Mar. 2006.

[4] Y. Huang, Z. Zhu, B. Guo, H. Lin, and S. Fang, "Design and thermal analysis on high torque low speed fractional-slot concentrated windings in-wheel traction motor," in *Proc. 22nd Int. Conf. Electr. Mach. (ICEM)*, 2016, pp. 1487–1492.

[5] F. Libert and J. Soulard, "Investigation on pole-slot combinations for permanent-magnet machines with concentrated windings," in *Proc. Int. Conf. Elect. Mach. (ICEM)*, 2004, pp. 5–8.

[6] E. Carraro, N. Bianchi, S. Zhang, and M. Koch, "Design and performance comparison of fractional slot concentrated winding spoke type synchronous motors with different slot-pole combinations," *IEEE Trans. Ind. Appl.*, vol. 54, no. 3, pp. 2276–2284, May/Jun. 2018.

[7] H. Dogan, F. Wurtz, A. Foggia, and L. Garbuio, "Analysis of slot-pole combination of fractional-slots PMSM for embedded applications," in *Proc. Int. Aegean Conf. Elect. Mach. Power Electron. Electromotion, Joint Conf.*, 2011, pp. 611–615.

[8] X. Zhu and M. Cheng, "Design and analysis of 10 MW class HTS exciting double stator direct-drive wind generator with stationary seal," *IEEE Access*, vol. 7, pp. 51129–51139, 2019.

[9] X. Ge and Z. Q. Zhu, "Sensitivity of manufacturing tolerances on cogging torque in interior permanent magnet machines with different slot/pole number combinations," *IEEE Trans. Ind. Appl.*, vol. 53, no. 4, pp. 3557–3567, Jul./Aug. 2017.

[10] L. Wu, R. Qu, and D. Li, "Reduction of rotor eddy-current losses for surface pm machines with fractional slot concentrated windings and retaining sleeve," *IEEE Trans. Magn.*, vol. 50, no. 11, pp. 1–4, Nov. 2014.

[11] M. Qiao, C. Jiang, Y. Zhu, and G. Li, "Research on design method and electromagnetic vibration of six-phase fractional-slot concentrated-winding PM motor suitable for ship propulsion," *IEEE Access*, vol. 4, pp. 8535–8543, 2016.

[12] I. Petrov, P. Lindh, M. Niemelä, E. Scherman, and J. Pyrhönen, "High-torque-density IPMSM rotor pole geometry adjustment for smooth torque," *IEEE Access*, vol. 7, pp. 52650–52658, 2019.

[13] S.-U. Chung, J.-M. Kim, D.-H. Koo, B.-C. Woo, D.-K. Hong, and J.-Y. Lee, "Fractional slot concentrated winding permanent magnet synchronous machine with consequent pole rotor for low speed direct drive," *IEEE Trans. Magn.*, vol. 48, no. 11, pp. 2965–2968, Nov. 2012.

[14] B. Dotz, M. Ippisch, and D. Gerling, "Design considerations on a 36-slot 28-pole permanent magnet drive," in *Proc. IEEE 12th Int. Conf. Power Electron. Drive Syst. (PEDS)*, Dec. 2017, pp. 360–367.

[15] A. M. El-Refaie and T. M. Jahns, "Scalability of surface PM Machines with concentrated windings designed to achieve wide speed ranges of constant-power operation," *IEEE Trans. Energy Convers.*, vol. 21, no. 2, pp. 362–369, Jun. 2006.

[16] S. G. Min and B. Sarlioglu, "Analysis and comparative study of flux weakening capability in fractional-slot concentrated windings," *IEEE Trans. Energy Convers.*, vol. 33, no. 3, pp. 1025–1035, Sep. 2017.

[17] D. Ishak, Z. Q. Zhu, and D. Howe, "Comparison of PM brushless motors, having either all teeth or alternate teeth wound," *IEEE Trans. Energy Convers.*, vol. 21, no. 1, pp. 95–103, Mar. 2006.

[18] F. Wu, P. Zheng, L. Cheng, and C. Zhou, "Analysis and experimental evaluation of harmonic leakage inductance for polyphase PM machines having close slot and pole combinations," *IEEE Trans. Magn.*, vol. 51, no. 11, pp. 1–4, Nov. 2015.

[19] P. Ponomarev, P. Lindh, and J. Pyrhonen, "Effect of slot-and-pole combination on the leakage inductance and the performance of tooth-coil permanent-magnet synchronous machines," *IEEE Trans. Ind. Electron.*, vol. 60, no. 10, pp. 4310–4317, Oct. 2013.

[20] C. M. Donaghy-Spargo, B. C. Mecrow, and J. D. Widmer, "On the influence of increased stator leakage inductance in single-tooth wound synchronous reluctance motors," *IEEE Trans. Ind. Electron.*, vol. 65, no. 6, pp. 4475–4482, Jun. 2018.

[21] J. Cros and P. Viarouge, "Synthesis of high performance PM motors with concentrated windings," *IEEE Trans. Energy Convers.*, vol. 17, no. 2, pp. 248–253, Jun. 2002.

[22] N. Bianchi, S. Bolognani, M. D. Prè, and G. Grezzani, "Design considerations for fractional-slot winding configurations of synchronous machines," *IEEE Trans. Ind. Appl.*, vol. 42, no. 4, pp. 997–1006, Jul./Aug. 2006.

[23] R. Krall, J. Krenn, and A. Schmid, "Comparison of leakage inductance between fractional slot winding and distributed winding," in *Proc. 16th Int. Power Electron. Motion Control Conf. Expo.*, 2014, pp. 276–282.

[24] P. Ponomarev, Y. Alexandrova, I. Petrov, P. Lindh, E. Lomonova, and J. Pyrhonen, "Inductance calculation of tooth-coil permanent-magnet synchronous machines," *IEEE Trans. Ind. Electron.*, vol. 61, no. 11, pp. 5966–5973, Nov. 2014.

[25] A. Taieb Brahimi, A. Foggia, and G. Meunier, "End winding reactance computation using a 3D finite element program," *IEEE Trans. Magn.*, vol. 29, no. 2, pp. 1411–1414, Mar. 1993.

[26] O. Chiver, E. Micu, and C. Barz, "Stator winding leakage inductances determination using finite elements method," in *Proc. 11th Int. Conf. Optim. Elect. Electron. Equip.*, 2008, pp. 69–74.

[27] T. A. Lipo, *Analysis of Synchronous Machines*. Boca Raton, FL, USA: CRC Press, 2012.

[28] D. W. Novotny and T. A. Lipo, *Vector Control and Dynamics of AC Drives*. Oxford, U.K.: Clarendon, 1996.

[29] S. M. Raziee, O. Misir, and B. Ponick, "Winding function approach for winding analysis," *IEEE Trans. Magn.*, vol. 53, no. 10, pp. 1–9, Oct. 2017.

ZICHONG ZHU (S'15) received the B.S. degree in thermal energy and power engineering from the Nanjing Institute of Technology (NJIT) and the M.S. degree in electrical engineering from Southeast University (SEU), Nanjing, China, where he is currently pursuing the Ph.D. degree with the School of Electrical Engineering.

His research interests include electromagnetic analysis, thermal simulation and structural design of permanent magnet synchronous machines for wheel-hub driving, wind power generation, and servo applications.

YUNKAI HUANG received the M.Sc. and Ph.D. degrees in electrical engineering from Southeast University, Nanjing, China, in 2001 and 2007, respectively, where he is currently a Professor with the School of Electrical Engineering.

His research interests include design and control of permanent magnet (PM) machine and high-speed brushless machine, applications in domestic appliances, electric vehicles, and wind-power generation systems.

JIANNING DONG (S'10–M'17) received the B.S. and Ph.D. degrees in electrical engineering from Southeast University, Nanjing, China, in 2010 and 2015, respectively. Since 2016, he has been an Assistant Professor with the Delft University of Technology (TU Delft), Delft, The Netherlands. Before joining TU Delft, he was a Postdoctoral Researcher with the McMaster Automotive Resource Centre (MARC), McMaster University, Hamilton, ON, Canada. His main research interests include design, modeling, and control of electromechanical systems.

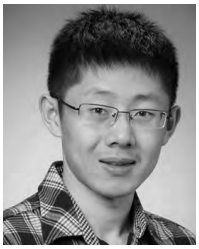

FEI PENG (S'15–M'16) received the B.S. and M.S. degrees in electrical engineering from Southeast University, Nanjing, Jiangsu, China, in 2010 and 2012, respectively, and the Ph.D. degree in electrical and computer engineering from McMaster University, Hamilton, ON, Canada, in 2016. He was a Postdoctoral Fellow with the McMaster Institute for Automotive Research and Technology (MacAUTO), McMaster University. In 2016, he joined the School of Electrical Engineering, Southeast University, as an Assistant Professor. His research interests include optimal design and control of power converters, and modeling and digital control of motor drives.